Journal of Fluorescence (2019) 29:61–73
https://doi.org/10.1007/s10895-018-2311-7

ORIGINAL ARTICLE

Nonlinear Optical Chromophores with Aggregation Induced Emission Enhancement Based on 2-N,N-Dibutylamino-4-Phenyl Thiazole with FMR Characteristics

Manali Rajeshirke[1] · Dharit Shah[1] · Nagaiyan Sekar[1]

Received: 28 August 2018 / Accepted: 14 October 2018 / Published online: 30 October 2018

Abstract

The synthesis, photophysical, linear and nonlinear optical (NLO) properties of novel fluorescent styryls based on 2-N,N-dibutylamino-4-phenyl thiazole as donor attached to different acceptor groups via conjugated π-bridge were studied with the help of solvatochromic model. The NLO properties of extended styryls based on benzylidene malononitrile and isophorone were more enhanced than the simple styryls based on malononitile and ethylcyano acetate which was attributed to the longer conjugation path. The benzylidene based extended styryl dye showed maximum value of two-photon absorption cross section σ_{2PA} 98.85GM in dichloromethane. The 2-amino thiazole derivatives were responsive towards the viscosity of the medium hence investigated for the fluorescent molecular rotor (FMR) properties wherein almost 2.07 to 3.65 fold increase in emission intensity was observed. Also, the aggregates of these dyes in N,N-dimethyl formamide-water mixture showed enhancement in emission on aggregates formation like 3.73 fold increase in emission intensity was observed for benzylidene based extended styryl dye. Thus NLOphoric AIEgens with FMR properties emitting in the red region of the electromagnetic radiation were developed.

Keywords 2-N,N-dibutylamino-4-phenyl thiazole · Aggregation induced emission (AIE) · Florescent molecular rotors (FMR) · Two-photon absorption

Introduction

Styryl dyes usually comprise of D-π-A design with variety of applications as sensitizers in photographic industry [1, 2], and the fluorescent ones are used in high tech applications like electroluminescence devices [3], optical signal processing [2, 4], nonlinear optics [5, 6]. The ease of synthesis, structure flexibility make them popular. NLO behavior of styryls is studied widely by substituting different donor and acceptor groups. 2-Aminothiazoles are important intermediates for disperse dyes, for example in the synthesis of commercially available monoazo C.I. Disperse Blue 339, a dye based on 2-amino-5-nitrothiazole and is widely studied [7, 8]. Substituted 2-aminothiazoles serve as important intermediate in synthesis of various drugs, as a coupler in azo dyes [9–17]. In our present research, we focus on novel styryls obtained from 2-N,N-dibutylamino-4-phenyl thiazole acting as donor attached via π-bridge of varying length with different acceptors. The fluorophore with long alkyl chain are sensitive towards the microenvironment especially the viscosity of the medium as the molecular rotations are directly dependent on the viscosity [18, 19]. Such fluorophores which are sensitive towards viscosity are known as Fluorescent molecular rotors (FMRs) and are used as viscosity measuring probes in several biological systems, and polymerization processes [20, 21]. Especially the FMRs with red emission are of current interest to have background free detection of biomolecules or viscosity of biofluids in biological systems. Also, another phenomena known as aggregation induced enhancement in emission (AIEE) observed in molecules with low or minimal fluorescence in dilute solution emit strongly when they aggregate [22]. The AIEE could be because of several reasons like restriction of intramolecular rotation (RIR), planarization, E/Z isomerization [23], twisted intramolecular charge transfer (TICT), restriction of

Electronic supplementary material The online version of this article (https://doi.org/10.1007/s10895-018-2311-7) contains supplementary material, which is available to authorized users.

✉ Nagaiyan Sekar
n.sekar@ictmumbai.edu.in

[1] Department of Dyestuff Technology, Institute of Chemical Technology, Nathalal Parekh Marg, Matunga, Mumbai 400 019, India

intramolecular vibration (RIV) and restriction of intramolecular motion (RIM) [24]. Thus AIEE is one of the contemporary topics of interest.

In our research here we explore the synthesis, characterization, viscosity sensitivity, AIEE property and NLO properties of the novel styryls from 2-N,N-dibutylamino-4-phenyl thiazole. The aldehyde of 2-N,N-dibutylamino-4-phenyl thiazole on Knoevenagel condensation with different active methylene resulted in formation of STD 1–4. The FMR, AIEE and NLO properties are studied for these dyes with help of simple spectroscopic data. The extended styryls STD 3–4 show enhanced properties compared to the simple styryls STD 1–2 and serve as NLOphore with additional functionality.

Experimental

Materials and Methods

The chemicals reagents were procured from Merck and SD Fine Chemical Limited, India. Progress of the reaction were monitor by thin layer chromatography (TLC) precoated plates of 0.25 mm E-Merck silica gel 60 F254. Recrystallization and column chromatography were used to purify the synthesized dyes. Standard melting point apparatus from Sunder Industrial Products, Mumbai was used to measure the melting points. 1H NMR and 13C NMR spectra were recorded on Agilent 500 MHz NMR instrument where TMS was used as an internal standard. The Perkin Elmer Lambda 25 UV visible spectrophotometer was used to record the absorption and further Varian Cary Eclipse fluorescence spectrophotometer was used to measure the emission of the synthesized compounds.

Synthesis and Characterization

The raw material 2-N,N-dibutylamino-4-phenyl thiazole was produced by known sequence of reactions [12, 25–29]. The purity of the compound was >80% and accordingly all the reactions were carried out. The 2-aminothiazole styryls STD 1–4 were synthesized via Knoevenagel condensation of 2-(dibutylamino) 4-phenylthiazole 5-carbaldehyde with active methylene compounds. The malononitrile, ethylcyanoacetate were commercially available whereas the 1a and 1b (Scheme 1) were obtained by the reported method [30–32]. The dyes were purified by column chromatography and characterized by melting point, 1H, 13C NMR spectroscopy, and elemental analysis.

Synthesis of 2-(Dibutylamino) 4-Phenylthiazole 5-Carbaldehyde Std_{carb}

Std_{carb} aldehyde was obtained from Vilsmeier–Haack formylation reaction. $POCl_3$ (41.9 mmol, 3.9 ml) was added dropwise in N,N-dimethyl formamide (4 ml) at 0 °C, to which the solution of 2-N,N-dibutylamino-4-phenyl thiazole (36 mmol, 1 eq) in N,N-dimethyl formamide at 0 °C was added further. This reaction mixture was stirred for 30 min at room temperature and then refluxed for 4 h. TLC was used to check the progress of the reaction. On completion of the reaction water is added to the mixture and neutralized with 2 N sodium bicarbonate solution. The product was extracted in chloroform and concentrated to obtain the green viscous liquid which solidified on cooling. Yield 60% M.pt. 38–40 °C. The aldehyde is condensed with the active methylenes to obtain the 2-amino thiazole styryls STD1–4.

General Procedure for the Synthesis of STD 1–4

A mixture of 2-(dibutylamino) 4-phenylthiazole 5-carbaldehyde Std_{carb} (1.3 ml, 4 mmol) and corresponding active methylene (5.5 mmol) in anhydrous ethanol (10 ml), and catalytic amount of piperidine was refluxed with constant stirring. The reaction progress was checked by TLC. The pure product was obtained by column chromatography using Petroleum Ether: Ethyl Acetate as eluent.

2-((2-(Dibutylamino)-4-Phenylthiazol-5-Yl) Methylene) Malononitrile STD 1

Color: Bright Yellow solid, Yield: 78%, M.pt. 87–90 °C. ^{1}H NMR (500 MHz, $CDCl_3$) δ 7.62 (s, 1H), 7.55–7.49 (m, 5H), 3.76 (t, 2H), 3.51–3.38 (m, 2H), 1.71 (dd, 4H), 1.41 (s, 4H), 0.99 (t, 6H). ^{13}C NMR (126 MHz, $CDCl_3$) δ 173.42 (s), 169.04 (s), 149.36 (s), 133.09 (s), 130.54 (s), 129.81 (s), 128.87 (s), 116.24 (d, J = 17.7 Hz), 115.02 (s), 67.54 (s), 20.03 (s), 13.79 (s). Anal. Calcd. for $C_{21}H_{24}N_4S$: C, 69.20; H, 6.64; N, 15.37%. Found: C, 69.23; H, 6.63; N, 15.39%.

Ethyl (E)-2-Cyano-3-(2-(Dibutylamino)-4-Phenylthiazol-5-Yl) Acrylate STD 2

Colour: Light Orange solid, Yield: 64%, M.pt. 62–65 °C. ^{1}H NMR (500 MHz, $CDCl_3$) δ 8.26 (s, 1H), 7.59 (dt, 2H), 7.50–7.46 (m, 3H), 4.27 (q, 2H), 3.64 (dd, 4H), 1.71 (dt, 4H), 1.44–1.36 (m, 4H), 1.32 (t, 3H), 0.98 (t, 26H). ^{13}C NMR (126 MHz, $CDCl_3$) δ 173.02 (s), 167.81 (s), 164.46 (s), 146.34 (s), 133.76 (s), 129.94 (d, J = 11.6 Hz), 128.64 (s), 117.45 (s), 115.93 (s), 90.52 (s), 77.34 (s), 77.08 (s), 76.83 (s), 62.98 (s), 61.63 (s), 29.34 (s), 24.74 (s), 20.05 (s), 14.30 (s), 13.83 (s). Anal. Calcd. for $C_{23}H_{29}N_3O_2S$: C, 67.12; H, 7.10; N, 10.21%. Found: C, 67.14; H, 7.11; N, 10.23%.

Scheme 1 Synthesis Strategy

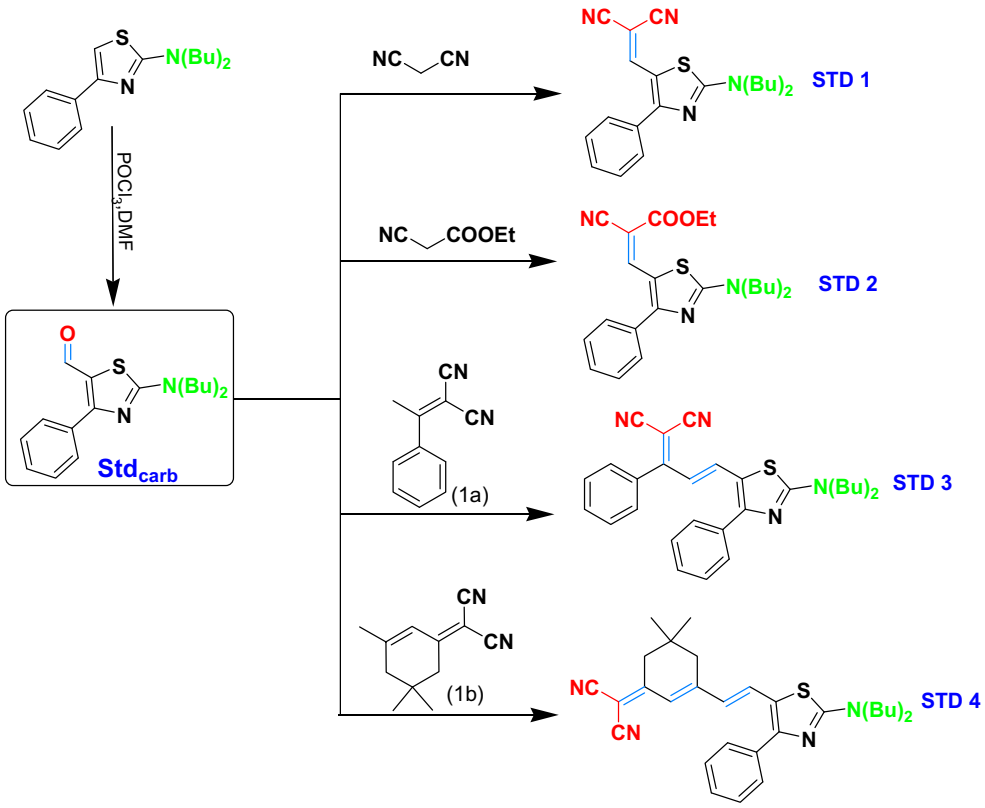

(E)-2-(3-(2-(Dibutylamino)-4-Phenylthiazol-5-Yl) -1-Phenylallylidene) Malononitrile STD 3

Colour: Grey solid, Yield: 41%, M.pt. 140–144 °C. ^{1}H NMR (500 MHz, $CDCl_3$) δ 7.46 (dd, 3H), 7.41–7.38 (m, 2H), 7.34–7.27 (m, 5H), 7.10 (d, 1H), 6.79 (d, J = 14.5 Hz, 1H), 3.64–3.47 (m, 4H), 1.77–1.66 (m, 4H), 1.47–1.36 (m, 4H), 1.00 (t, 6H). ^{13}C NMR (126 MHz, $CDCl_3$) δ 171.04 (s), 170.65 (s), 162.54 (s), 141.37 (s), 133.88 (d, J = 6.2 Hz), 130.44 (s), 129.37 (d, J = 16.6 Hz), 128.68 (d, J = 4.1 Hz), 128.28 (s), 119.77 (s), 119.41 (s), 114.93 (s), 114.37 (s), 29.38 (s), 20.10 (s), 13.85 (s). Anal. Calcd. for $C_{29}H_{30}N_4S$: C, 74.64; H, 6.48; N, 12.01%. Found: C, 74.67; H, 6.47; N, 12.02%.

2-(3-((E)-2-(2-(Dibutylamino)-4-Phenylthiazol-5-Yl) Vinyl)-5, 5-Dimethylcyclohex-2-Enylidene)-2-Isocyanoacetonitrile *STD 4*

Colour: Dark Grey solid, Yield: 35%, M.pt. 175–182 °C. ^{1}H NMR (500 MHz, $CDCl_3$) δ 7.60 (d, J = 7.4 Hz, 2H), 7.43 (dt, J = 26.3, 7.3 Hz, 3H), 7.25–7.19 (m, 2H), 6.66 (s, 1H), 6.33 (d, J = 15.2 Hz, 1H), 3.54–3.44 (m, 4H), 2.51 (s, 2H), 2.26 (s, 2H), 1.72–1.64 (m, 4H), 1.38 (dq, J = 14.8, 7.4 Hz, 4H), 1.03–0.94 (m, 12H). ^{13}C NMR (126 MHz, $CDCl_3$) δ 168.60 (d, J = 10.2 Hz), 157.05 (s), 154.91 (s), 135.03 (s), 129.63 (s), 129.29 (s), 128.65 (d, J = 25.1 Hz), 128.50–128.38 (m), 126.00 (s), 121.12 (s), 120.50 (s), 114.38 (s), 113.61 (s), 51.30 (s), 42.88 (s), 38.96 (s), 31.96 (s), 29.43 (s), 27.97 (s), 20.10 (s), 13.88 (s). Anal. Calcd. for $C_{30}H_{36}N_4S$: C, 74.34; H, 7.49; N, 11.56%. Found: C, 74.35; H, 7.48; N, 11.57%.

Results and Discussion

Design of Styryls STD1–4

2-N,N-Dibutylamino-4-phenyl thiazole styryl derivatives with D-π-A framework having various electron acceptor groups are synthesized by Knovenagel condensation and are characterized by ^{1}H NMR, ^{13}C NMR, CHN analysis and UV-Vis spectroscopy. The five membered thiazole ring plays a vital role while designing series of styryl molecules by adding planarity to the molecule. We have synthesized STD 1–2 which are simple styryls whereas STD 3–4 are extended styryls. As expected the extended styryls show better optical properties than the simple ones. Also these styryls have low melting point due to the presence of butyl chain in the structure.

Absorption and Emission Properties

The optical properties of 5 μM solution of all the styryls were examined in various microenvironment at 25 °C and values were charted in Table 1. All the styryls absorb in the wavelength range of 442 to 544 nm. The order of absorption is STD

Table 1 Experimental optical properties of STD 1–4 in various solvents

Dye	Solvent	$\lambda^{abs(a)}$	$\lambda^{emi(b)}$	$\Delta\upsilon^{(c)}$		$\varepsilon_{max}{}^{(d)}$	$\Phi_f{}^{(e)}$	$f^{(f)}$	$K_r{}^{(g)}$	$K_{nr}{}^{(h)}$	$\sigma_1(\upsilon)^{(i)}$ (cm^2)
				cm^{-1}	nm						
STD 1	Toluene	442	503	2743.72	61	16340	0.0005	2.27	9.80	19,600.00	6.24
	DCM	446	506	2658.68	60	19100	0.0046	2.50	9.7	2100.00	7.30
	Acetonitrile	442	508	2939.40	66	20000	0.0032	2.63	9.30	2900.00	7.64
	Methanol	442	502	2704.12	60	19280	0.0030	2.53	8.70	2880.00	7.37
	DMSO	450	509	2575.86	59	17980	0.0059	2.35	0.11	1850.00	6.87
	DMF	446	510	2813.68	64	18300	0.0004	2.45	0.11	27,800.00	6.99
STD 2	Toluene	438	499	2790.97	61	8020	0.0330	1.10	5.00	147.00	3.06
	DCM	442	503	2743.72	61	11380	0.0032	1.52	6	1870.00	4.35
	Acetonitrile	438	502	2910.73	64	12720	0.0210	1.72	5.80	272.00	4.86
	Methanol	492	502	404.88	10	787.34	0.0260	0.13	52.00	19.60	3.01
	DMSO	444	498	2442.20	54	14160	0.0390	1.89	8.6	211.00	5.41
	DMF	442	497	2503.71	55	13240	0.0630	1.78	7.50	111.00	5.06
STD 3	Toluene	510	579	2336.69	69	5960	0.0080	0.89	4.10	521.00	2.27
	DCM	524	592	2192.08	68	8040	0.0130	1.20	5.40	406.00	3.07
	Acetonitrile	514	592	2563.36	78	7840	0.0100	1.20	3.70	365.00	2.99
	Methanol	512	588	2524.45	76	7700	0.0130	1.21	3.70	277.00	2.94
	DMSO	530	595	2061.20	65	2880	0.0250	0.41	1.50	57.70	1.10
	DMF	524	598	2361.56	74	2660	0.0350	0.41	1.60	43.50	1.01
STD 4	Toluene	530	623	2816.56	93	14750	0.0350	0.32	98.00	27.00	5.63
	DCM	540	651	3157.54	111	10750	0.0990	0.20	46.00	4.17	4.11
	Acetonitrile	526	654	3720.89	128	11000	0.0800	0.23	42.00	4.83	4.20
	Methanol	530	657	3647.22	127	12750	0.0910	0.27	50.00	5.04	4.87
	DMSO	544	663	3299.40	119	13250	0.1310	0.26	36.00	2.42	5.06
	DMF	540	667	3526.01	127	12750	0.2190	0.25	53.00	1.87	4.87

[a] the wavelength with maximum absorption in nm

[b] the wavelength with maximum emission intensity in nm

[c] Stokes Shift in cm^{-1} and nm

[d] absorptivity in L M^{-1} cm^{-1}

[e] quantum yield

[f] oscillator strength

[g] radiative rate constant ($\times 10^{-8}$ s^{-1})

[h] non-radiative rate constant ($\times 10^{-8}$ s^{-1}), and

[i] absorption cross section in ($\times 10^{-20}$ cm^2)

2(442 nm) > STD 1(446 nm) > STD 3 (524 nm) > STD 4 (540 nm) in dichloromethane. The dyes STD 1–4 have D-π-A framework with different acceptor groups and π conjugation length which tunes the photophysical properties of the dyes. The absorption spectra and emission spectra of the dyes are presented in Figs. 1 and 2. As observed in Table 1 there is not much difference in the absorption maxima of dyes STD 1 and STD 2, whereas it significantly increases in case of extended styryls STD 3 and STD 4 which is attributed to increase in conjugation chain and better intramolecular charge transfer. The STD 1 shows little bathochromic compared to STD 2 due to presence of stronger dicynovinyl acceptor than ethyl cyanoethoxycarbonyl. Similarly, for STD 3 and STD 4 as the π system increases red shift is absorption maxima is observed. The absorption spectra for simple styryls STD 1 and STD 2 are least affected by the solvent polarity, whereas for the extended styryls STD 3 and STD 4 increase of 14-20 nm is observed with rise in polarity of solvent from toluene to N,N-dimethyl formamide (DMF) (Table 1).

Red shift in fluorescence emission is observed in order: STD 2(503 nm) > STD 1(506 nm) > STD 3 (592 nm) > STD 4 (651 nm) in dichloromethane. As observed in absorption spectra the solvatochromism is more enhanced in case of extended styryls STD 3 and STD 4 than simple styryls STD 1 and STD 2. In extended styryls, a 20-44 nm bathochromic shift is observed from non-polar toluene to polar DMF (Table 1). In extended styryls, the Stokes shift increases with rise in solvent polarity, for example in STD 4 Stokes shift is 93 nm in toluene which increases to 127 nm in methanol. Also a blue shift in absorption and emission spectra in polar protic solvent like methanol was observed for all the styryls STD 1–4 compared to polar aprotic solvents like DMF due to the hydrogen bond interactions of solvent with the N, N, dibutyl amine donor of solute thereby decreasing the donor capacity and decrease in ICT characteristics leading to blue shifted absorption and emission. Thus from the results, it is predicted that strong acceptor and increase in π conjugation resulted in bathochromic shift in both the absorption and emission

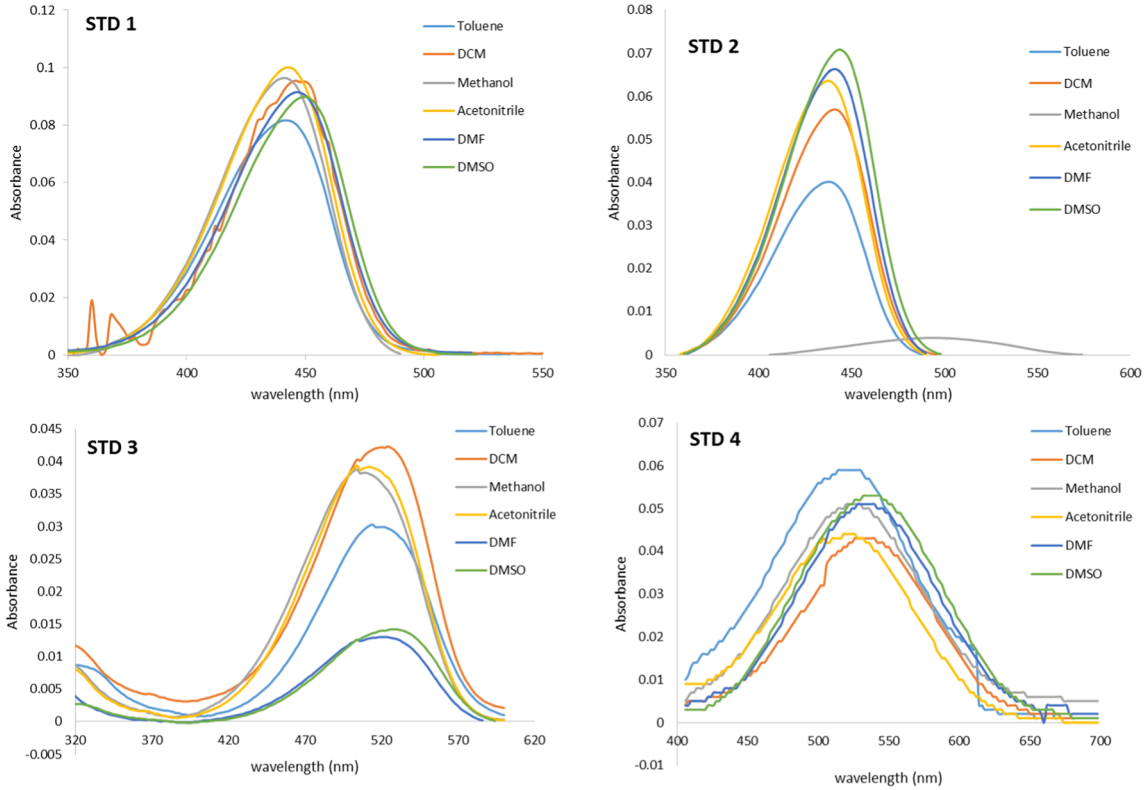

Fig. 1 Absorption plot of STD 1–4 in different solvents

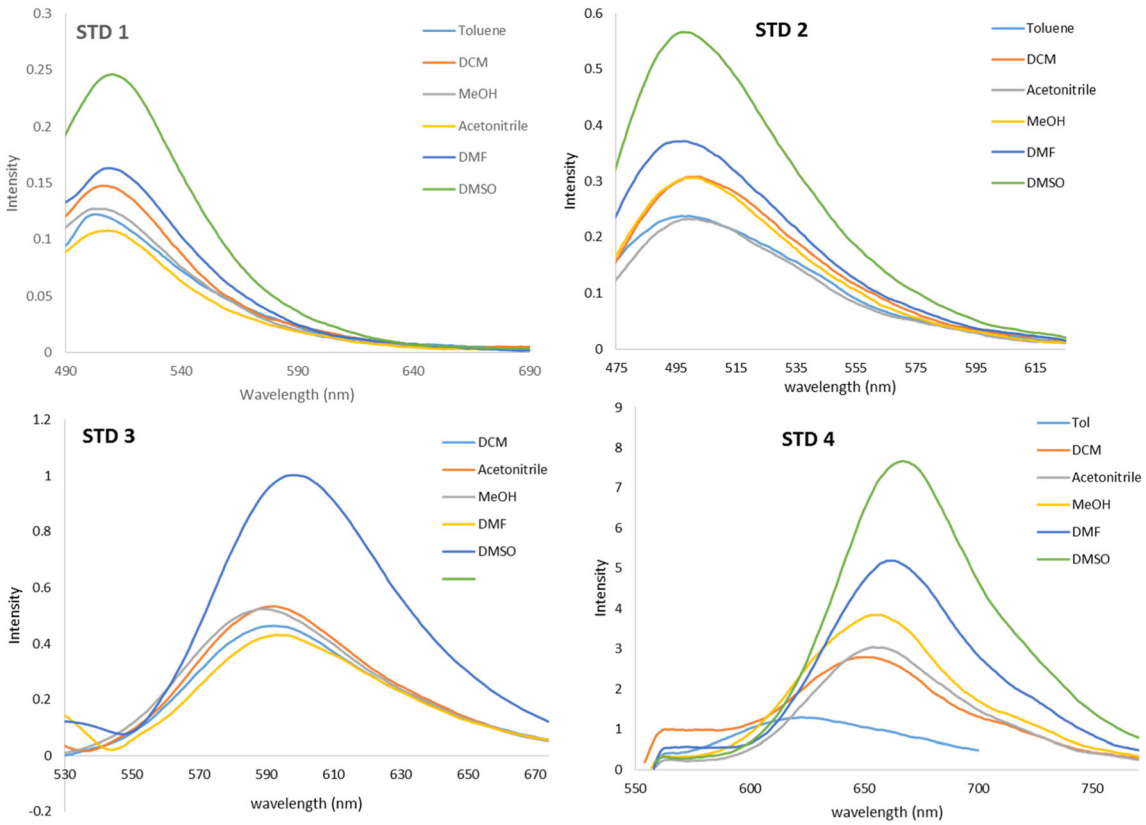

Fig. 2 Emission plot of STD 1–4 in different solvents

properties. The quantum yield in solvents were measured for all the dyes using Rhodamine 6G as reference standard and presented in Table 1. Higher quantum yield is seen in polar solvents like DMF than in non-polar solvent for all the dyes. All the dyes show overall low quantum yield indicative of more non-radiative relaxation than radiative relaxation as best explained by the study of radiative and non-radiative radiative rate constant of the dyes.

Radiative and Non-radiative Rate Constant

According to Stickler Berg the radiative (K_r) and non-radiative rate constants in all the studied solvent is given by the Eqs. (1) and (2);

$$K_r = 2.88 \times 10^{-9} n^2 \frac{\int_{\Delta \upsilon_e} f(\bar{\upsilon})}{\int_{\Delta \upsilon_a} f(\bar{\upsilon}) \bar{\upsilon}^{-3} d\bar{\upsilon}} \int \epsilon(\bar{\upsilon}) d\bar{\upsilon} \tag{1}$$

$$K_{nr} = \frac{1-\phi_F}{\tau} \tag{2}$$

Wherein the $\Delta \upsilon_a$ and $\Delta \upsilon_e$ represents the experimental limits of absorption and emission bands (S_0–S_1 transitions) respectively, the molar extinction coefficient as ϵ, the wavenumber (cm^{-1}) as $\bar{\upsilon}$ and $f(\bar{\upsilon})$ as the maximum fluorescence intensity measured in atomic unit (a.u.) and τ fluorescence lifetime. The K_r, and K_{nr} values for STD1–4 were analyzed using Eqs. 1 and 2 and charted in Table 1. It is clearly observed that the K_{nr} values are greater than the K_r resulting into lower quantum yields as the decay of excited state occur via non-radiative pathways. As observed in Table 1 the extended styryls STD 3–4 are more responsive towards solvents. For STD 3–4 the K_{nr} values are higher in nonpolar solvent like toluene than in polar solvents whereas the K_r and Φ_F values are higher in polar solvents than in nonpolar solvents (Table 1). This behavior in extended styryls is attributed to strong solvation of the solute molecules by the polar solvent molecules thus restricting the non-radiative relaxation pathways and increasing the K_r and Φ_F values in polar solvent.

Solvatochromism and Charge Transfer (CT) Characteristics

The extended thiazole styryls STD 3–4 showed more emission solvatochromism than absorption solvatochromism, whereas very minimum to negligible solvatochromism is seen for simple styryls STD 1–2. Thus the CT characteristics with the help of polarity functions is studied for STD 3 and 4 only. As observed in Table 1 there is increase in Stokes shift of the STD 3–4 in polar solvent compared to nonpolar solvents due to polar excited state in polar solvent. Thus the CT characteristics of STD 3–4 can be better understood from the study excess dipole moment obtained from the polarity function plots Lippert-Mataga [33], McRae [34], and Bakhshiev [35]. The Lippert-Mataga (LM) theory states CT characteristic as;

$$\bar{\upsilon}_{abs} - \bar{\upsilon}_{emn} = \left(\frac{1}{4\pi\epsilon_O}\right)\left(\frac{2\left(\mu_e - \mu_g\right)^2}{hca^3}\right) f_{LM} + Constant \tag{3}$$

where Lippert-Mataga (LM) function is given as;

$$f_{LM}(\varepsilon, n) = \frac{\varepsilon - 1}{2\varepsilon + 1} - \frac{n^2 - 1}{2n^2 + 1} \tag{4}$$

where $\bar{\upsilon}_{abs} - \bar{\upsilon}_{emn}$ is the Stokes shift (in cm^{-1}), h represents Planck's constant (in erg x s), c is the speed of light in vacuum (in cm s^{-1}), "a" as Onsager radius (in cm), ε represents the relative dielectric constant, and n as static refractive index of solvent. The LM function also known as orientation polarizability behaves linearly against the Stokes shift with good regression coefficient for the synthesized dyes in studied solvents indicates the influence of that polarity and polarizability factors of solvent onto the absorption and emission of STD 3–4 (Fig. 3).

McRae equation

$$\bar{\upsilon}_{abs} - \bar{\upsilon}_{emn} = \left(\frac{1}{4\pi\epsilon_O}\right)\left(\frac{2\left(\mu_e - \mu_g\right)^2}{hca^3}\right) f_{McRae} + Constant \tag{5}$$

where McRae function is given as;

$$f_{McRae}(\varepsilon, n) = \frac{\varepsilon - 1}{\varepsilon + 2} - \frac{n^2 - 1}{n^2 + 2} \tag{6}$$

Furthermore improved version of LM is McRae model is studied wherein the McRae function ($f_{McRae}(\varepsilon,\eta)$) is given by Eq. 6, the plot of f_{McRae} versus Stokes shift also showed a good linear relation for STD 3–4. Thus, the linearity in LM and MacRae plots for STD 3–4 shows that the CT occur from local excited state.

Weller's equation

$$\vartheta_{emn} = \frac{2(\mu_e)^2}{hca^3} f_w + constant \tag{7}$$

where Weller's function $f_w(\varepsilon, n)$ is given as;

$$f_w(\varepsilon, n) = \frac{\varepsilon - 1}{2\varepsilon + 1} - \frac{n^2 - 1}{4n^2 + 2} \tag{8}$$

Along with the LM and McRae model, the Weller's model was also implied in order to study the charge transfer from in the D-π-A styryls. The Weller's plot considers only the emission maxima vs the $f_w(\varepsilon, n)$ which was linear for STD 3–4 with good regression coefficient indicative of ICT characteristics at excited state.

Dipole Moment Ratio

Further, the CT characteristics of STD 3–4 were studied from the excited to ground state dipole moment ratio and by the generalized Mulliken Hush (GMH) charge transfer analysis.

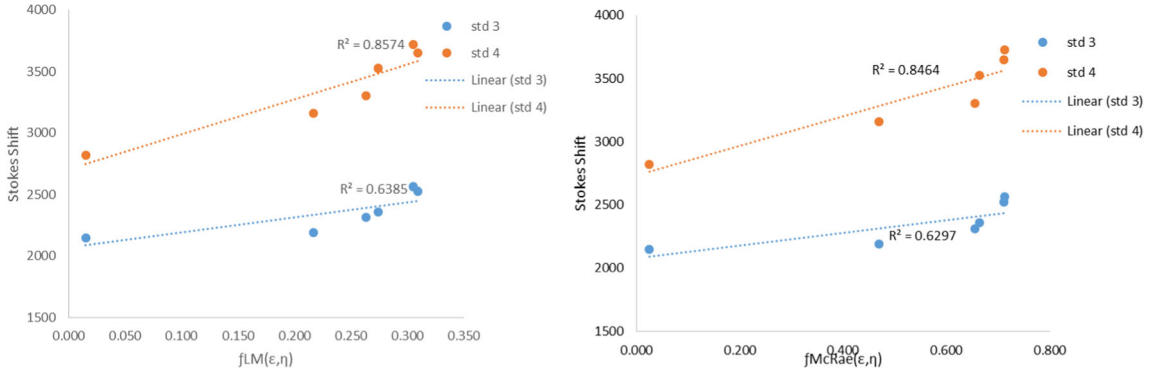

Fig. 3 Lippert-Mataga and McRae plot for STD 3–4

The excited to ground state dipole moment of the dye is responsive towards the microenvironment of the dye. The relations between the polarity functions based on the relative permittivity (ε) and refractive index (η) of the solvents with the spectroscopic data help in the study the excited state dipole moment of the dyes. Thus by using Bilot-Kawski [36], Bakhshiev [35] and Liptay [37, 38] polarity functions plots the ratio of excited state to the ground state dipole moment μ_e/μ_g for STD 3–4 is calculated and listed in Table 2, the detailed equations are provided in the supporting information. The ratio of μ_e/μ_g is larger than unity in some cases while near to unity in a few other cases, suggestive of a more polar excited state than the ground state in STD 3–4.

Mulliken-Hush Charge Transfer Analysis

The two-state model based Generalized Mulliken-Hush (GMH) analysis is also studied for STD 3–4 to understand the CT characteristic. In this method the strength of electronic coupling (H_{DA}) is calculated using spectroscopic data and expressed by Eq. 9 [39–41];

$$H_{DA} = \frac{\mu_{ge}\Delta E_{eg}}{\Delta\mu_{eg}^{D}} = \frac{\mu_{ge}\Delta E_{eg}}{\left(\Delta\mu^2 + 4\Delta\mu_{ge}^2\right)^{1/2}} \tag{9}$$

which relates the electronic coupling H_{DA} strength between the ground (S_0) and CT excited states with the vertical excitation energy (ΔE_{eg}). $\Delta\mu_{eg}$ denotes the difference between the adiabatic dipole moments of the ground and excited states and $\Delta\mu^{D}_{eg}$ as the difference in diabatic state dipole moments.

Three diabatic states – a donor ground state (GS), a donor locally excited state (LE), and a charge-transfer state (CT) with the "transferring electron" localized on the acceptor constitutes the adiabatic states, which is studied well in CT systems [42, 43]. The center to center separation distance (R_{DA}) in Å is calculated using following Eq. (10) from the molar absorptivity (ε_{max}), bandwidth ($\Delta\bar{\upsilon}_{1/2}$) and ΔE_{eg} as;

$$R_{DA} = 2.06 \times 10^{-2} \frac{\left(\Delta E_{eg} \times \varepsilon_{max} \times \Delta\bar{\upsilon}_{1/2}\right)^{1/2}}{H_{DA}} \tag{10}$$

$$C_b^2 = \frac{1}{2}\left(1 - \left(\frac{\Delta\mu^2}{\Delta\mu_{eg}^{D}}\right)^2\right)^{1/2} \tag{11}$$

Similarly, the eq. (11) shows the degree of delocalization or fractional degree of localization of the excess charge (C_b^2). The values of H_{DA}, R_{DA}, and C_b^2 for STD 3–4 were calculated using Eqs. (9–11) and listed in Table 3. When C_b^2 is zero it represents the state with total delocalization and total localization of charge is seen for C_b^2 approaches to unity. The C_b^2 values of STD 3–4 indicates a good operative ICT characteristics in the dye (Table 3). Also, the R_{DA} for both the dyes is less in polar solvent which is even supported by the bathochromic shift on polarity rise (Table 3). These dyes along with good charge transfer characteristics were also responsive towards environment, thus viscosity sensitivity and AIEE study was employed.

Table 2 Excited to ground state dipole moment ratio $\left(\frac{\mu_e}{\mu_g}\right)$ of STD 3–4

	STD 3	STD 4
Bilot-Kawski	0.83	3.48
Bakhshiev	3.18	0.87
Liptay	4.14	0.98

Table 3 Generalized Mulliken-Hush charge transfer analysis values for STD 3–4 in different solvents

Solvent	STD 3			STD 4		
	C_b^2	H_{DA} (cm^{-1})	R_{DA} (^0A)	C_b^2	H_{DA} (cm^{-1})	R_{DA} (^0A)
Toluene	0.4903	9638	2.32	0.4754	9166	2.93
DCM	0.4918	9483	2.25	0.4699	8944	2.91
Acetonitrile	0.4918	9669	2.45	0.4718	9208	2.81
Methanol	0.4917	9705	2.35	0.4746	9172	2.87
DMSO	0.4861	9462	2.39	0.4729	8905	2.60
DMF	0.4860	9442	2.33	0.4731	8981	2.81

Viscosity Sensitivity of STD 1–4 in Non-polar Aprotic (Toluene-Paraffin) Solvent Mixtures

The emission quantum yield in non-polar solvent for STD 1–4 was very low (Table 1) indicative of radiationless relaxation pathway more preferable in coming back from excited state by the molecule. This can be due to molecular rotations occurring within the molecule which favors the relaxation of excited state in non-radiative way like by diminishing the fluorescence by collisions. Thus viscosity of the medium plays a vital role in enhancing the fluorescence intensity by obstructing the molecular rotations indirectly decreasing the possibility of non-radiative relaxation. Herein effect of viscosity is studied in toluene and paraffin solvent mixtures where the viscosity of the medium is increased by increasing the paraffin liquid volume and its effect on fluorescence emission intensity is observed. The Fig. 4 represents the enhancement of fluorescence intensity of 10 μM solution of STD1–4 in different solvent mixtures 10 to 100% of paraffin. The increase in emission intensity for STD 1 is 3.65 fold, STD 2 is 2.07, STD 3 is 3.40 and STD 4 is 3.0 fold (Fig. 4). Thus the synthesized styryls act as FMR especially the extended styryls can act red emitting FMR which could be useful for biological applications.

Aggregation Enhanced Emission Study

The dyes STD1–4 were subjected to AEE experiments. The molecular structure, presence of chromophore, and restricted intramolecular rotations (RIR) affect the AEE effect. In condensed phase the fluorophores experience RIR which lead to enhancement in emission intensity. The 50 μM solution of STD 1–4 in N, N-dimethyl formamide/water solvent mixtures with varying compositions ranging from 0% to 95% water with same dye concentration were examined by fluorescence spectroscopy (Fig. 5). Water is a bad solvent and thus induces the aggregates formation. The dyes in pure solvent have low emission intensity but as we increase the fraction of water the aggregates formation enhances the fluorescence intensity due to RIR factor. But further increase after certain fraction of water, however, the fluorescence intensity decreases gradually this could be attributed to increase in intermolecular stacking of aggregates. From Fig. 5 for STD 1 and 2 the emission intensity enhances till 90% water fraction further increase led to decrease in emission intensity. Similarly, for STD 3, the fluorescence intensity increases till 80% water fraction and for STD 4 it was till 70% water fraction, further decrease in emission intensity was observed with increase in water fraction (Fig. 5). Thus the STD 1–4 show AEE phenomena in DMF/water mixture.

NLO Properties Computed by Solvatochromic Method

The push-pull styryls with D-π-A design usually possess NLO properties owing to their efficient CT characteristics operative between the end groups [44, 45]. Sophisticated techniques are used to measure the NLO properties like Electric Field Induced Second Harmonic Generation (EFISH)

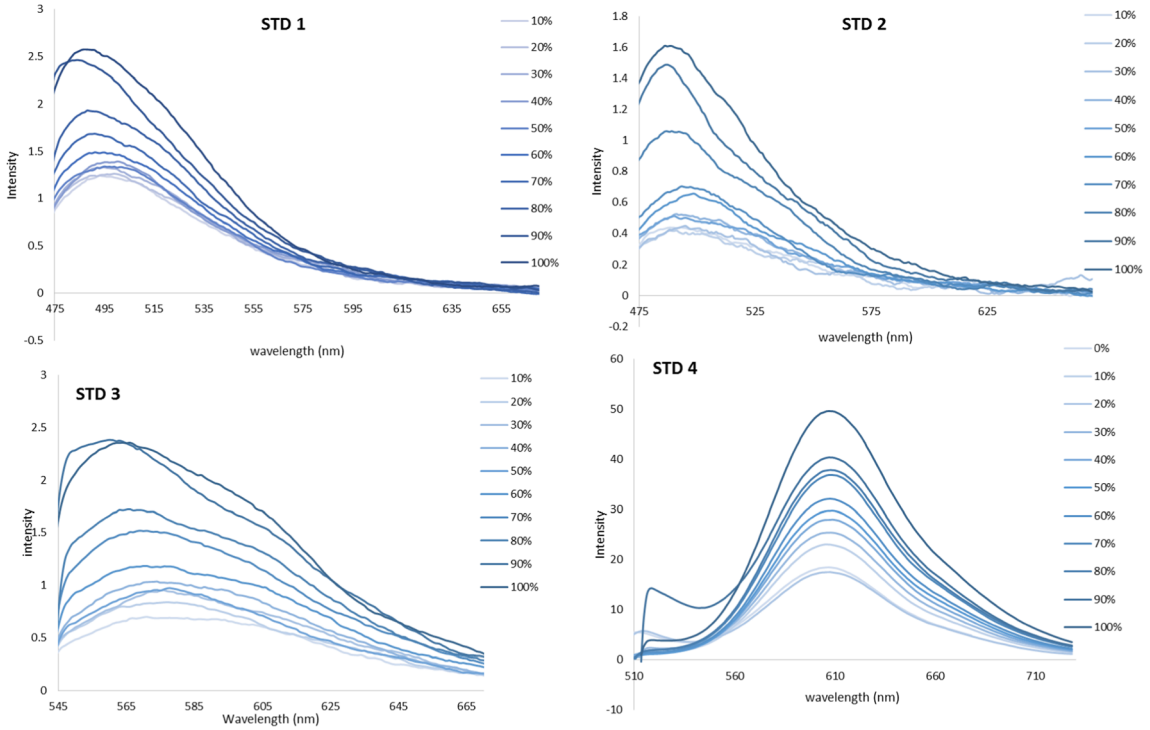

Fig. 4 Viscosity sensitivity of 10 μM solution of STD 1–4 in Toluene-Paraffin mixture of varying viscosity

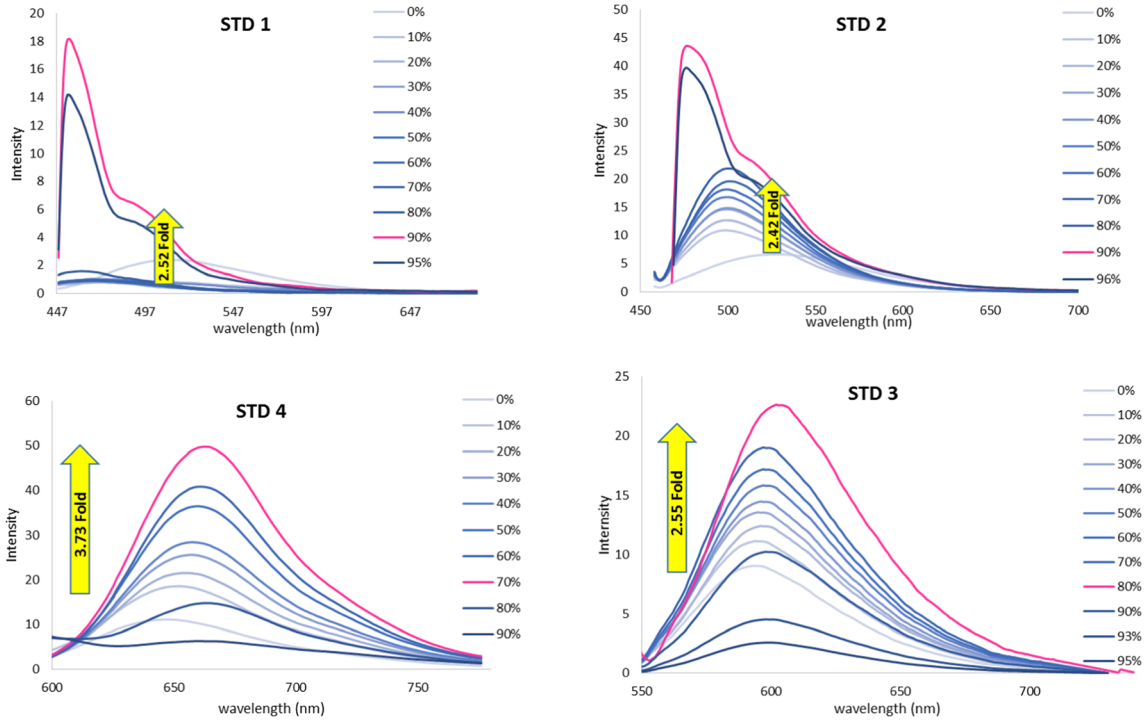

Fig. 5 AEE of 50 μM solution of STD 1–4 in DMF-Water mixture of varying % of water

technique at 1907 nm fundamental wavelength, hyper-Rayleigh scattering (HRS) often at 1064 nm which are expensive [2]. So herein we have employed simple solvatochromic method which uses the spectroscopic data to evaluate the NLO properties which help in primary screening of NLOphores before approaching to the sophisticated techniques. The solvatochromic model is grounded on two-level microscopic model wherein the linear polariizabilty (α_{CT}), hyperpolarizability (β_{CT}), second hyperpolarizability (γ_{SD}) and two photon absorption cross section (σ_{2PA}) is obtained for STD 1–4 in the studied solvents.

Linear Polarizability (α_{CT})

The linear polarizability α_{CT} from two level model is expressed by Eq. (12), where the direction of CT is given by x, the Plank's constant is given by h, c as the velocity of light in vacuum, λ_{eg} is the wavelength of transition from the ground state to excited state, transition dipole moment,μ_{eg} which is calculated from the oscillator strength obtained from spectroscopic data, and thus the Eq. (12)is as;

$$\alpha_{CT} = \alpha_{xx} = 2\frac{\mu_{ge}{}^2}{\Delta E_{eg}} = \frac{2\mu_{eg}{}^2\lambda_{eg}}{hc} \tag{12}$$

Thus the α_{CT} values for STD 1–4 were evaluated using Eq. (12) in different solvents and listed in Table 4. From Table 4 for STD 1–4 the α_{CT} values are less in non-polar solvents toluene, while higher in polar solvents DMF. The order of α_{CT} among the dyes is STD1 > STD2 > STD3 > STD4 which is directly proportional to the donor-acceptor strength and conjugation length. As the conjugation length increase as in case of extended styryls, there is decrease in the polarizability values compared to the simple styryls. Also among the simple styryls, the STD 1 has stronger acceptor dicynovinyl group compare to STD 2 thus α_{CT} of STD 1 is higher than STD 2.

Hyperpolarizability (β_{CT})

The Oudar equation founded on two level model for evaluation of hyperpolarizability (β_{CT}) in different microenvironments is given as [46–48],

$$\beta_{CT} = \frac{3}{2h^2c^2}\ \frac{\upsilon_{eg}{}^2\mu_{eg}{}^2\Delta\mu_{CT}}{\left(\upsilon_{eg}{}^2-\upsilon_L{}^2\right)\left(\upsilon_{eg}{}^2-4\upsilon_L{}^2\right)} \tag{13}$$

where transition frequency denoted as $v_{eg,}$ $\Delta\mu_{CT}$ which is the excited and ground state dipole moment difference is obtained from the McRae's theory, the reference incident radiation frequency to which β is referred is denoted as v_L, h as the Planck's constant, speed of light as c in cm s^{-1}, and transition dipole moment as $\mu_{eg.}$ As the solvatochromism is seen only for the extended styryls STD 3–4, linearity in McRae plot is seen only for extended styryls, and thus $\Delta\mu_{CT}$ and hyperpolarizability are calculated for STD 3–4 only.

The hyperpolarizability calculated from Eq. (13) is with dominant tensor component in the CT direction thus also

Table 4 Linear Polarizability α_{CT} of STD 1–4 in different solvents obtained by solvatochromic model

Property	Solvent	STD 1	STD 2	STD 3	STD 4
α_{CT} (cm^{-1})	Toluene	9.48923E-23	4.53173E-23	4.96103E-23	1.94391E-23
	DCM	1.06782E-22	6.38002E-23	7.03228E-23	1.27368E-23
	Acetonitrile	1.0992E-22	7.07692E-23	6.65398E-23	1.34929E-23
	Methanol	1.05994E-22	6.76154E-24	6.69741E-23	1.62535E-23
	DMSO	1.02174E-22	7.99875E-23	2.41806E-23	1.63439E-23
	DMF	1.04651E-22	7.43475E-23	2.41583E-23	1.54329E-23

referred as β_{xxx} or $\beta_{CT.}$ When excitation $v_L = 0$ the static hyperpolarizability is presented as;

$$\beta_{xxx} = \beta_{CT} = \frac{3}{2}\frac{{\mu_{eg}}^2 \Delta\mu_{CT}}{\left({E_{eg}}^2\right)} \tag{14}$$

Thus by substituting the values of $\Delta\mu_{CT}$ and μ_{eg} obtained from the spectroscopic data in the above equation the values of β_{CT} or β_{xxx} is obtained in different solvents and listed in Table 5. The value of β_{CT} for STD 3 is 32.93×10^{-30}esu and 21.86×10^{-30}esu for STD 4 in toluene. Also, the value of β_{CT} for both the dyes decreases with increase solvent polarity. The CT characteristics of STD 3 is more than that of STD 4 as evident from the higher β_{CT} value which is due to the presence of phenyl ring adding to aromaticity of the dye while in case of STD 4 though the length of conjugation is more the aromatic character is less than in STD 3 resulting in lowering of CT and low $\beta_{CT.}$ The β_{CT} values calculated by solvatochromic model though based on several assumptions allowing only approximate estimation of dominant tensor $\beta_{CT,}$ it helps in understanding the trend of hyperpolarizability before approaching to other expensive sophisticated methods.

Second Order Hyperpolarizability $\langle\gamma\rangle_{SD}$

The second order hyperpolarizability $\langle\gamma\rangle_{SD}$ for STD 3–4 is evaluated at molecular level with the help of three-level model [47, 49–51] using transition dipole moment $\mu_{eg,}$ difference between ground- and excited-state dipole moments, which in simpler form presented by Eq. (15) [49, 52];

$$<\gamma> \propto \left(\frac{1}{\Delta {E_{eg}}^3}\right) {\mu_{eg}}^2 \left(\Delta {\mu_{eg}}^2 - {\mu_{ge}}^2\right) \tag{15}$$

The value,

$$\left(\frac{1}{{E_{eg}}^3}\right) {\mu_{eg}}^2 \left(\Delta\mu^2 - {\mu_{eg}}^2\right) \tag{16}$$

Symbolizes the trend in the third order hyperpolarizability and also designated as the "solvatochromic descriptor". The

Table 5 NLO properties of STD 3–4 in different solvents obtained by solvatochromic model

Dye	Solvent	μ^2_{ge} [a]	σ_{2PA} [b]	β_{CT} [c]	γ_{SD} [d]
STD 3	Toluene	9.68828E-35	94.14	3.2926E-29	1.98351E-35
	DCM	1.33385E-34	98.85	4.94665E-29	3.09085E-35
	Acetonitrile	1.31218E-34	96.25	4.29957E-29	2.51682E-35
	Methanol	1.32074E-34	94.80	4.4182E-29	2.63011E-35
	DMSO	4.59524E-35	44.24	1.72277E-29	1.07588E-35
	DMF	4.58223E-35	39.03	1.69531E-29	1.05678E-35
STD 4	Toluene	3.64539E-35	65.67	2.18619E-29	2.18399E-35
	DCM	2.34428E-35	43.52	1.43583E-29	1.4378E-35
	Acetonitrile	2.54955E-35	38.21	1.44704E-29	1.37851E-35
	Methanol	3.04798E-35	42.01	1.72716E-29	1.63031E-35
	DMSO	2.98606E-35	60.84	1.88227E-29	1.92557E-35
	DMF	2.84052E-35	51.68	1.7113E-29	1.68561E-35

[a] Square of Transition dipole moment in esu.cm

[b] Two photon absorption cross-section in GM

[c] first hyperpolarizability β_{CT} in esu, and

[d] second hyperpolarizability γ_{SD} in esu

calculated values for STD 3–4 in studied solvents is presented in Table 5. The $\langle\gamma\rangle_{SD}$ for STD 3 is 10.75×10^{-36}esu and 19.25×10^{-36}esu for STD 4 in DMSO which is many fold higher than the value for urea (0.68×10^{-36} esu).

Two Photon Absorption Cross-Section (σ_{2PA})

The two-level system can also be employed for polar unsymmetrical molecules with either parallel or antiparallel dipole moments to get the two-photon absorption cross-section (σ_{2PA}) as given by Eq. (17) as;

$$\sigma_{2PA} = \frac{2(2\pi L)^4}{5(hcn)^2}\left(\Delta\mu_{eg}\right)^2 \mu_{ge}^2 g(2\upsilon) \tag{17}$$

$L = \frac{(n^2+2)}{3}$, where L is known as the Lorentzian local field factor, n represents the refractive index of the solvent used. The difference between excited and ground state dipole moments $\Delta\mu_{eg}$ and transition dipole $\mu_{eg}$is obtained from spectroscopic data. The term $\mu_{10}^2 g(2\upsilon)$ wherein g(2υ) is the normalized TPAb line shape function can be expressed as;

$$\mu_{10}^2 g(2\upsilon) = \mu_{10}^2 g(\upsilon_{10}) = \frac{3 \times 10^3 ln10h}{(2\pi)^3 N_A}\left(\frac{\varepsilon_{abs}}{\upsilon_{emi}}\right)$$

TPAb line shape is assumed to be approximated by the OPA line shape using spectroscopic properties like the molar extinction coefficient, dipole moment as follow [53];

$$\sigma_{2PA} = \frac{12\ln 10\,\pi 10^3 L^4}{15 N_A h c^2 n^2}\left(\Delta\mu_{eg}\right)^2\left(\frac{\varepsilon_{abs}}{\upsilon_{emi}}\right) \tag{18}$$

$$\sigma_{2PA} = 4.84 \times 10^{-15}\frac{L^4}{n^2}\left(\Delta\mu_{eg}\right)^2\left(\frac{\varepsilon_{abs}}{\upsilon_{emi}}\right) \tag{19}$$

Thus σ_{2PA} can be obtained from steady state absorption and emission measurements wherein the $\Delta\mu_{eg}$ is obtained from the slope of Onsager's polarity function (f_{OF}) plot against Stokes shift. Onsagar polarity equation is given as

$$\bar{\upsilon}_{abs} - \bar{\upsilon}_{emn} = \left(\frac{1}{4\pi\epsilon_O}\right)\left(\frac{2\left(\mu_e - \mu_g\right)^2}{hca^3}\right) f_{OF} + Constant \tag{20}$$

$f_{OF} = \frac{2((\epsilon-1)}{2\epsilon+1}$, where ϵ is the Dielectric Constant of the solvent.

The σ_{2PA} values of STD 3–4 are evaluated using Eq. (19) and presented in Table 5. As observed the dye with greater molar extinction coefficient, and larger one-photon cross section (OPA) has larger σ_{2PA}. The dye STD 3 has larger σ_{2PA} than STD 4 which is due to more aromatic character of STD 3 attributable to the presence of phenyl ring. The aromaticity is hindered a bit in case of STD 4 even though π-conjugation length is more which is attributed to the presence of non-aromatic isophorone ring. Thus the density of electron cloud is less in STD 4 than STD 3 leading to overall decrease in the CT characteristics of the dye and hence the NLO properties of the same. The σ_{2PA} values for STD 3–4 obtained from the two state model though overestimated as many assumptions are considered in the model [53], the solvatochromic two level model serves as good tool to understand the basic trend in the NLO properties at lower cost.

Conclusion

We have successfully synthesized novel group of 2-N,N-dibutylamino-4-phenyl thiazole styryls via Knoevenagel condensation and were well characterized by ^{1}H NMR, ^{13}C NMR, CHN analysis and UV-Vis spectroscopy. The extended styryls STD 3–4 showed superior optical properties than the simple styryls STD 1–2 owing to the strong acceptor and increase in conjugation length. The overall quantum yields of STD1–4 is low. In particular the quantum yield in extended styryls STD 3–4 is more in polar aprotic solvents DMF than in non-polar solvents which is due to the strong solvation of the solute molecules by the polar solvent molecules thus restricting the non-radiative relaxation pathways and increasing the K_r and ϕ_F values in polar solvent. The extended styryls STD 3–4 showed good charge transfer characteristics as evident form the dipole moment ratio and Mulliken-Hush charge transfer analysis. The dyes were responsive towards environment, thus viscosity sensitivity and AIEE study was employed. The STD 1–4 showed 2–3.65 fold increase in emission intensity, thus these styryls can be used as red emitting FMR which could be useful for biological applications. Also the STD 1–4 show AEE phenomena in DMF/water mixture. The linear and NLO properties of the dyes were studied with the help of solvatochromic model where the extended styryls STD 3–4 showed enhanced properties than the STD 1–2. Among the STD 3–4, the STD 3 showed better NLO properties than STD 4 due to more charge transfer characteristic. Thus we have successfully developed multi-functional NLOphoric 2-aminothiazole based styryls.

Acknowledgements The author Manali Rajeshirke is thankful to University Grants Commission and Dharit Shah to Technical Education Quality Improvement Program, Ministry of Human Resource Development, Government of India for financial support.

References

1. Lu M, Zhu Y, Ma K, Cao L, Wang K (2012) Spectrochimica Acta part a : molecular and biomolecular spectroscopy facile synthesis and photo-physical properties of cyano-substituted styryl derivatives based on carcarbazole/phenothiazinepectrochim. Acta Part A Mol Biomol Spectrosc 95:128–134. https://doi.org/10.1016/j.saa.2012.04.090

2. Barsella A, Yalçın E, Achelle S et al (2015) Styryl-based NLO chromophores : synsynthesis, spectroscopic properties, and theoretical calculations. Tetrahedron Lette 56:2586–2589
3. Wang B, Wang Y, Hua J, Jiang Y, Huang J, Qian S, Tian H (2011) Starburst triarylamine donor-acceptor-donor quadrupolar derivatives based on cyano-substituted diphenylaminestyrylbenzene: tunable aggregation-induced emission colors and large two-photon absorption cross sections. Chem - A Eur J 17:2647–2655. https://doi.org/10.1002/chem.201002821
4. Rajeshirke M, Katariya SB, Sekar N (2017) Carbazole-based mono and Bis-styryl NLOphores: structure property correlations. J Solut Chem 46:2109–2129. https://doi.org/10.1007/s10953-017-0691-y
5. Yordanova S, Petkov I, Stoyanov S (2014) Solvatochromism of homodimeric styryl pyridinium salts. J Chem Technol Metall 49: 601–609
6. Jedrzejewska B, Krawczyk P, Pietrzak M et al (2013) Styryl dye possessing donor-pi-acceptor structure - synthesis, spectroscopic and computational studies. Dyes Pigments 99:673–685. https://doi.org/10.1016/j.dyepig.2013.06.008
7. Maradiya HR, Patel VS (2001) Thiazole based disperse dyes for nylon and polyester fibers. Fibers Polym 2:153–158. https://doi.org/10.1007/BF02875329
8. Maradiya HR (2012) Disperse dyes based on 2-aminothiazole derivatives for cellulose triacetate fabric. J Saudi Chem Soc 16:69–74. https://doi.org/10.1016/j.jscs.2010.10.021
9. Babu BH, Vijay K, Murali Krishna KB et al (2016) An efficient PEG-400 mediated catalyst free green synthesis of 2-aminothiazoles from α-diazoketones and thiourea. J Chem Sci 128: 1475–1478. https://doi.org/10.1007/s12039-016-1130-0
10. Zarnegar Z, Safari J (2016) Magnetic carbon nanotube-supported imidazolium cation-based ionic liquid as a highly stable nanocatalyst for the synthesis of 2-aminothiazoles. Appl Organomet Chem 30:1043–1049. https://doi.org/10.1002/aoc.3540
11. Sadeghi M, Safari J, Zarnegar Z (2016) Synthesis of 2-aminothiazoles from methylcarbonyl compounds using a Fe3O4 nanoparticle-: N -halo reagent catalytic system. RSC Adv 6: 64749–64755. https://doi.org/10.1039/c6ra11175k
12. Safari J, Abedi-Jazini Z, Zarnegar Z, Sadeghi M (2016) Nanochitosan: a biopolymer catalytic system for the synthesis of 2-aminothiazoles. Catal Commun 77:108–112. https://doi.org/10.1016/j.catcom.2016.01.007
13. Dickey JB, Towne EB, Bloom MS, Moore WH, Hill HM, Heynemann H, Hedberg DG, Sievers DC, Otis MV (1959) Azo dyes from substituted 2-Aminothiazolesl. J Org Chem 24:187–196. https://doi.org/10.1021/jo01084a010
14. Chen B, Zhao R, Wang B et al (2010) A new and efficient preparation of 2-aminothiazole-5-carbamides : applications to the synthesis of the anti-cancer drug. ARKIVOC 2010:32–38
15. Das D, Sikdar P, Bairagi M (2016) Recent developments of 2-aminothiazoles in medicinal chemistry. Eur J Med Chem 109:89–98
16. Yen MS, Chen CW (2010) The synthesis of vinyltriethoxysilane-modified heteroaryl thiazole dyes and silica hybrid materials. Dyes Pigments 86:129–132. https://doi.org/10.1016/j.dyepig.2009.12.006
17. Singh BS, Lobo HR, Krishna Podagatlapalli G, Venugopal Rao S, Shankarling GS (2013) Thiazole based novel functional colorants: synthesis, characterization and nonlinear optical studies using picosecond Z-scan technique. Opt Mater (Amst) 35:962–967. https://doi.org/10.1016/j.optmat.2012.11.018
18. Chipem FAS, Chatterjee S, Krishnamoorthy G (2010) Theoretical study on photochemical behavior of trans −2- [4 - (dimethylamino) styryl] benzothiazole. J Photochem Photobiol A Chem 214:121–127. https://doi.org/10.1016/j.jphotochem.2010.06.014
19. Pati AK, Gharpure SJ, Mishra AK (2014) Substituted diphenyl butadiynes: a computational study of geometries and electronic transitions using DFT/TD-DFT. Phys Chem Chem Phys 16: 14015–14028. https://doi.org/10.1039/c4cp00580e
20. Ibarra-Rodríguez M, Muñoz-Flores BM, Dias HVR et al (2017) Fluorescent molecular rotors of Organoboron compounds from Schiff bases: synthesis, viscosity, reversible Thermochromism, cytotoxicity, and bioimaging cells. J Org Chem 82:2375–2385. https://doi.org/10.1021/acs.joc.6b02802
21. Haidekker MA, Theodorakis EA (2010) Environment-sensitive behavior of fluorescent molecular rotors. J Biol Eng 4:1–14. https://doi.org/10.1186/1754-1611-4-11
22. Li L, Nie H, Chen M, Sun J, Qin A, Tang BZ (2017) Aggregation-enhanced emission active tetraphenylbenzene-cored efficient blue light emitter. Faraday Discuss 196:245–253. https://doi.org/10.1039/C6FD00163G
23. Wang L, Shen Y, Zhu Q, Xu W, Yang M, Zhou H, Wu J, Tian Y (2014) Systematic study and imaging application of aggregation-induced emission of Ester-Isophorone derivatives. J Phys Chem C 118:8531–8540. https://doi.org/10.1021/jp412279m
24. Padalkar VS, Sakamaki D, Kuwada K, Tohnai N, Akutagawa T, Sakai KI, Seki S (2016) AIE active triphenylamine–benzothiazole based motifs: ESIPT or ICT emission. RSC Adv 6:26941–26949. https://doi.org/10.1039/C6RA02417C
25. Krasovskii VA, Burmistrov SI (1969) Alkylation of 2-Aminothiazole and 2-Amino-4-methylthiazole with tert-Butyl Alcohol. Chem Heterocycl Compd 5:46–48. https://doi.org/10.1007/BF01031760
26. Kaye IA, Parris CL (1952) Acylated 2-Iminothiazolines. J Org Chem 17:737–741. https://doi.org/10.1021/jo01139a011
27. Gillon DW, Forrest IJ, Meakins GD, Tirel MD, Wallis JD (1983) N, N-Disubstituted 2-aminothiazole-5-carbaldehydes: preparation and investigation of structural features. J Chem Soc Perkin Trans 1: 341–347. https://doi.org/10.1039/P19830000341
28. Gondi SR, Son DY (2008) Synthesis of (hetaryl)alkylamines from the reactions of 2-aminopyrimidine, 2-aminothiazole, and 2-aminothiazoline with benzyl bromide and xylylene dibromides. Synth Commun 38:401–410. https://doi.org/10.1080/00397910701771074
29. Cambia RC, Lee HH, Rutledge PS, Woodgate PD (1979) vic-Iodothiocyanates and iodoisothiocyanates. Part 2. New syntheses of thiazolidin-2-ones and 2-amino-2-thiazolines. J Chem Soc Perkin Trans 1:765–70. https://doi.org/10.1039/P19790000765
30. Cramer CJ, Truhlar DG (2009) Density functional theory for transition metals and transition metal chemistry. Phys Chem Chem Phys 11:10757–10816. https://doi.org/10.1039/b907148b
31. Dev P, Agrawal S, English NJ (2013) Functional assessment for predicting charge-transfer excitations of dyes in complexed state: a study of triphenylamine-donor dyes on titania for dye-sensitized solar cells. J Phys Chem A 117:2114–2124. https://doi.org/10.1021/jp306153e
32. Lanke SK, Sekar N (2016) Aggregation induced emissive carbazole-based push pull NLOphores: synthesis, photophysical properties and DFT studies. Dyes Pigments 124:82–92. https://doi.org/10.1016/j.dyepig.2015.09.013
33. Valeur B (2001) Molecular fluorescence principles and applications. Wiley-VCH, Weinheim. Analytical atomic spectrometry with flames and plasmas handbook of analytical techniques single-molecule detection in solution. Methods and Applications Methods. https://doi.org/10.1002/3527600248
34. McRae EG (1954) Theory of solvent effects on molecular electronic spectra. Frequency Shifts J Phys Chem 61:1957–1572. https://doi.org/10.1021/j150551a012
35. Bruni S, Cariati E, Cariati F, Porta FA, Quici S, Roberto D (2001) Determination of the quadratic hyperpolarizability of trans-4-[4-(dimethylamino)styryl]pyridine and 5-dimethylamino-1,10-phenanthroline from solvatochromism of absorption and fluorescence spectra: a comparison with the electric-field-induced second-harmon. Spectrochim Acta - Part A Mol Biomol Spectrosc 57:1417–1426. https://doi.org/10.1016/S1386-1425(00)00483-2

36. Kawski A (2002) On the estimation of excited-state dipole moments from solvatochromic shifts of absorption and fluorescence spectra. Zeitschrift fur Naturforsch - Sect A J Phys Sci 57:255–262. https://doi.org/10.1515/zna-2002-0509
37. Sworakowski J, Lipiński J, Ziółek Ł, Palewska K, Nešpůrek S (1996) Solvatochromism of a Zwitterionic Benzimidazole-based Pyridinium betaine dye: UV−Vis spectroscopic measurements and quantum-chemical calculations. J Phys Chem 100:12288–12294. https://doi.org/10.1021/jp960184x
38. Rettig W (1986) Charge separation in excited states of decoupled systems—TICT compounds and implications regarding the development of new laser dyes and the primary process of vision and photosynthesis. Angew Chemie Int Ed English 25:971–988. https://doi.org/10.1002/anie.198609711
39. Cave RJ, Newton MD (1996) Generalization of the Mulliken-hush treatment for the calculation of electron transfer matrix elements. Chem Phys Lett 249:15–19. https://doi.org/10.1016/0009-2614(95)01310-5
40. Cave RJ, Newton MD (1997) Calculation of electronic coupling matrix elements for ground and excited state electron transfer reactions: comparison of the generalized Mulliken–hush and block diagonalization methods. J Chem Phys 106:9213–9226. https://doi.org/10.1063/1.474023
41. Zheng J, Kang YK, Therien MJ, Beratan DN (2005) Generalized Mulliken-hush analysis of electronic coupling interactions in compressed π-stacked porphyrin-bridge-quinone systems. J Am Chem Soc 127:11303–11310. https://doi.org/10.1021/ja050984y
42. Gwaltney SR, Rosokha SV, Head-Gordon M, Kochi JK (2003) Charge-transfer mechanism for electrophilic aromatic nitration and nitrosation via the convergence of (ab initio) molecular-orbital and Marcus-hush theories with experiments. J Am Chem Soc 125:3273–3283. https://doi.org/10.1021/ja021152s
43. Tathe AB, Sekar N (2016) Red emitting NLOphoric 3-styryl coumarins: experimental and computational studies. Opt Mater (Amst) 51:121–127. https://doi.org/10.1016/j.optmat.2015.11.031
44. Ravikumar C, Joe IH, Jayakumar VS (2008) Charge transfer interactions and nonlinear optical properties of push-pull chromophore benzaldehyde phenylhydrazone: a vibrational approach. Chem Phys Lett 460:552–558. https://doi.org/10.1016/j.cplett.2008.06.047
45. Raimundo JM, Blanchard P, Gallego-Planas N, Mercier N, Ledoux-Rak I, Hierle R, Roncali J (2002) Design and synthesis of push-pull chromophores for second-order nonlinear optics derived from rigidified thiophene-based π-conjugating spacers. J Org Chem 67:205–218. https://doi.org/10.1021/jo010713f
46. Oudar JL, Chemla DS (1977) Hyperpolarizabilities of the nitroanilines and their relations to the excited state dipole moment. J Chem Phys 66:2664–2668. https://doi.org/10.1063/1.434213
47. Oudar JL (1977) Optical nonlinearities of conjugated molecules. Stilbene derivatives and highly polar aromatic compounds. J Chem Phys 67:446. https://doi.org/10.1063/1.434888
48. Momicchioli F, Ponterini G, Vanossi D (2008) First- and second-order polarizabilities of simple merocyanines. An experimental and theoretical reassessment of the two-level model. J Phys Chem A 112:11861–11872. https://doi.org/10.1021/jp8080854
49. Carlotti B, Flamini R, Kikaš I, Mazzucato U, Spalletti A (2012) Intramolecular charge transfer, solvatochromism and hyperpolarizability of compounds bearing ethenylene or ethynylene bridges. Chem Phys 407:9–19. https://doi.org/10.1016/j.chemphys.2012.08.006
50. Margar SN, Rhyman L, Ramasami P, Sekar N (2016) Fluorescent difluoroboron-curcumin analogs: an investigation of the electronic structures and photophysical properties. Spectrochim Acta - Part A Mol Biomol Spectrosc 152:241–251. https://doi.org/10.1016/j.saa.2015.07.064
51. Champagne B, Perpète ÉA, André J-M, Kirtman B (1997) Analysis of the vibrational static and dynamic second hyperpolarizabilities of polyacetylene chains. Synth Met 85:1047–1050. https://doi.org/10.1016/S0379-6779
52. Dirk CW, Cheng L-T, Kuzyk MG (1992) A simplified three-level model describing the molecular third-order nonlinear optical susceptibility. Int J Quantum Chem 43:27–36. https://doi.org/10.1002/qua.560430106
53. Rodrigues CAB, Mariz IFA, MaçÔas EMS et al (2012) Two-photon absorption properties of push-pull oxazolones derivatives. Dyes Pigments 95:713–722. https://doi.org/10.1016/j.dyepig.2012.06.005